Study of the Early Stages of Electrocrystallization of Zinc-Iron Alloy on E 24 Steel

Samia. Amirat[1], Karima. Abderrahim[2], Wahiba. Bouchelaghem [3].Rabah.Rehamnia[1],Juan. Creus[4]

[1]Nanomaterials Corrosion and Surface Treatment Laboratory (LNCTS), BadjiMokhtar University, B.P.12-23000, Annaba, Algeria.

[2]Surface Engineering Laboratory (L.I.S), BadjiMokhtar University, B.P.12-23000, Annaba, Algeria.

[3]Laboratory of Inorganic materials chemistry, University BadjiMokhtar Annaba, Algeria

[4]Laboratory Of Studies Of Materials In Mediums Aggressive, University La Rochelle, Avenue Michel Crépeau, F-17042 , Rochelle Cedex 0, France.

*Corresponding author: karima.abderrahim@univ-annaba.dz,samia.amirat@univ-annaba.dz

Recived: 28/05/2023; Revised: 20/10/2023; Accepted: 29/11/2023

Abstract

In this work, zinc-iron alloys were obtained by simple electroplating with imposed potential and from an acid chloride electrolyte in the presence of saccharin and glycerol as additives.

The deposition mechanism of the zinc-iron alloy has been described according to the Scharifker and Hills model.

The morphology of the obtained alloys was characterized by observations in SEM scanning electron microscopy; The results show that the imposed potential influences the electroplating mechanism, thus the morphology and corrosion resistance.

Keywords: Alloy, Electro-crystallization, Nucleation- growth, Zn-Fe, morphology, ALSV

*TobRegul Sci.™ 20 - -;9(2):*1475 - 1489

DOI: doi.org/10.18001/TRS.9.2.92

1. Introduction

Sacrificial zinc coating on steel and other iron substrates is an effective and reliable industry standard for corrosion protection. The elements that are used successfully for alloying with zinc are iron, cobalt, nickel and tin. The important functions of alloying elements iron group with zinc are usually used to preserve the sacrificial properties of zinc[1,2].

Zn-Fe alloy has attracted considerable attention, especially in the automotive industry because it combines high corrosion resistance with excellent mechanical performance and good compatibility with organic coatings.

These alloys replace toxic Cadmium-based coatings.

Acid baths showed a high current efficiency and better recovery rate, but have a low power launch.

The presence of additives in the bath has influenced the physical and mechanical properties of the coatings, such as grain size, structure, luminosity, internal stress, pitting and the chemical composition and corrosion behaviour.

Silva and al [3,4] deposited the Cu–Zn alloy coating on a mild steel substrate of a bath containing sodium citrate as a complexing agent, and benzotriazole and cysteine as additives.

Nucleation and growth is the most important stage in the metal plating process. The competition between nucleation and growth determines the particle size of the deposited metal[5]. The overall appearance and structure of the composite is determined by the shape of the crystal growth.

The first stage of the formation of a new phase on a different substrate is generally accepted by the three-dimensional (3D) nucleation and growth process and also by the adsorption reactions and formation of low dimensionality systems, preferentially localized inhomogeneous surfaces of substances[6].

In this study, electroplating of Zn–Fe alloys was performed using a chloride acid bath with saccharin and glycerol as an additive. The influence of the imposed potential saccharin on the electrocrystallization process and their early stages of nucleation and growth. Then assess the morphology and corrosion behaviour of coatings was carried out.

2. Procedure

2.1 Materials, electrolytes and methods

- Zn–Fe alloy electrodeposition was carried out in one cylindrical cell compartment maintained at 50°C. To prepare the solution, the following salts were used: $ZnCl_2$ 0.15 M, $FeCl_2$ 0.75 M, KCl 180g/L, acideborique 25g/L, 0.02 M acide L-ascorbique, brillanteur, 2g/L « Saccharine», 10^{-3} M « Glycérol».
- The electrochemical measurements were carried out using a potentiostat / galvanostat, brand voltalab PGZ 301, associated with a volta-master software and equipped with a classical electrochemical cell with three electrodes: reference electrode (Er) in saturated calomel (SCE), counter electrode in platinum and a working electrode (Et) in E24 steel. This last one is coated

in an epoxy resin delimiting a flat working surface of 0.5cm^2, successively polished with silicon carbide (SiC) abrasive papers at different granulometries: 800, 1200, 2400 and 4000.

- The deposition of the Zn–Fe alloys was performed at Imposed potential varying from -1300 to - 1500mV/Ag, AgCl.
- The anode linear dissolution ALSV (anode linear scanning voltametry) has been produced immediately after the synthesis of the deposits. All coatings are deposited at approximately

same thicknesses. An anode potential sweep at a speed of 20mV/s was then applied from the value of the abandonment potential of the coating until its complete dissolution.

Dissolution takes place in the same environment used for the production of coatings. When the coatings are anodically polarized components dissolve at different potentials depending on their morphology and structure.

Electrochemical measurements were made after 1h of immersion at 323K:

❖ The corrosion behaviour of the deposits was studied in a NaCl bath at 30 g/l. This chloride ion concentration is close to that of seawater, for which Zn-Fe alloys may be exposed.
❖ The polarization curves i(E) are drawn at 0.2 mV/s on a range of potential of + 0.25 V/Ag, AgCl around the abandonment potential, the curves are obtained after one hour of immersion in a saline environment.
❖ The impedance measurements of the steel deposits were carried out in potentiostatic mode, around corrosion potential, after varying immersion times. The frequency range studied from 100KHz to 10 mHz. The sinusoidal disturbance had a low amplitude (5mV).
❖ The chemical composition and morphology of the electrodeposits were characterized by a JEOL JSM-54 SIE Laboratory LA. ROCHELLE.

2. 2. Surface analysis

The surface morphology of the Zn-Fe alloys obtained in the absence and presence of saccharin was studied using a JEOL JSM-54 scanning electron microscope, coupled to an energy dispersive spectrometer (EDS).

3. Results and discussion

3.1 Influence of the imposed potential on the formation of Zn-Fe alloys.

According to Figure 1, the evolution of the current density over the electroplating time shows that the maximum appears at – 1300mV/Ag, AgCl.

Zn-Fe electroplating on vitreous carbon follows multiple nucleation (3D) with diffusion-controlled growth according to the Scharifker-Hills model[2, 7].

The transients were normalized to I^2/I^2max as a function of t/t max and then compared to the well-known theory of Sharifker and Hills.

The curve plots clearly show in figures III.2 and III.3 that the Zn-Fe alloy on E24 steel with potential -1300 mV/Ag, AgCl follows a theoretical response of an instantaneous nucleation the curve found by tracing the transients I^2/Im is similar to curve (a) Sharifker and Hills mod.

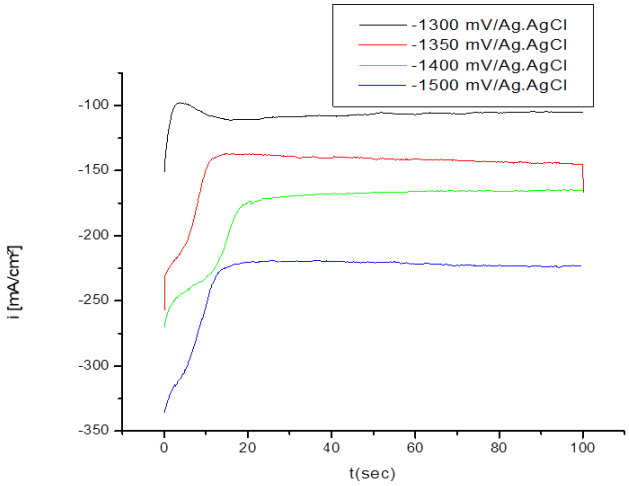

Fig.1.Influence of the imposed potential on the formation and dissolution of Zn-Fe alloys on vitreous carbon.

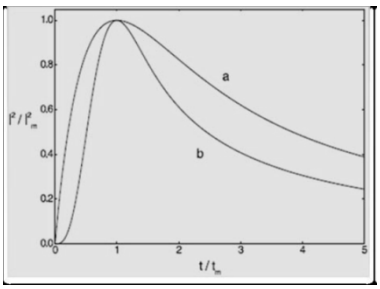

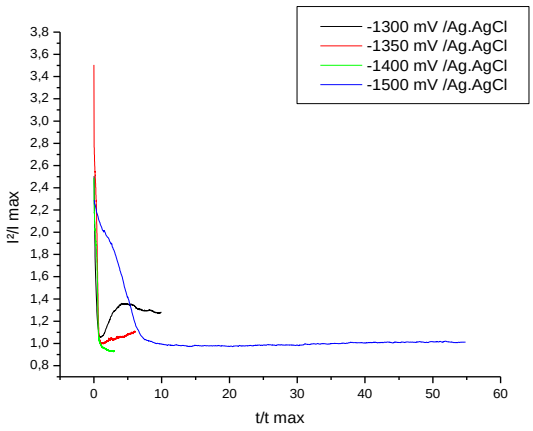

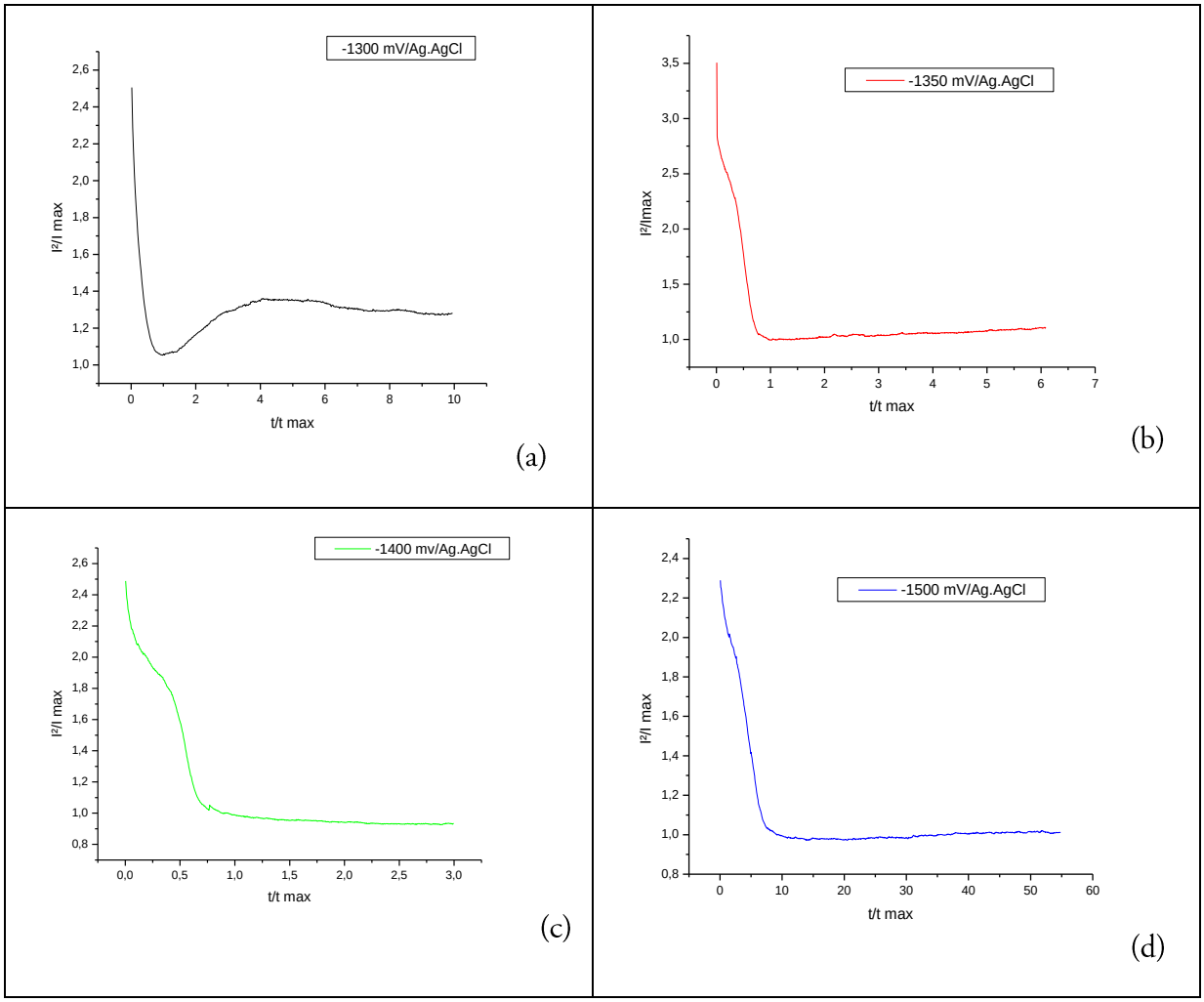

Fig.2.Fonction sans dimension I^2/Im en fonction de t/tm Electrodéposition du Zn-Fe à différents potentiels imposés.

3. 2. Influence of the imposed potential on the dissolution of Zn-Fe alloys.

ALSV anodic dissolutions of coatings deposited in electrolyte at different potentials (-1300 -1500 mV/Ag.AgCl) are shown respectively in Figure 3.

The shapes of the dissolution curves of coatings deposited from an electrolyte of ZnCl2 0.15 M, FeCl20.75 M, KCl 180g/L, acide borique 25g/L, 0.02 M acide L-ascorbique, brillanteur, 2g/L « Saccharine», 10^{-3} M « Glycérol». at 50°C are quite similar and these curves correspond to the dissolution of a single phase (a single step).

In addition, the electrochemical species involved in the dissolution of these coatings (width of the dissolution peak) are very similar, which means that their cathodic efficiencies are constant (quantity deposited/ theoretical quantity) [8,9].

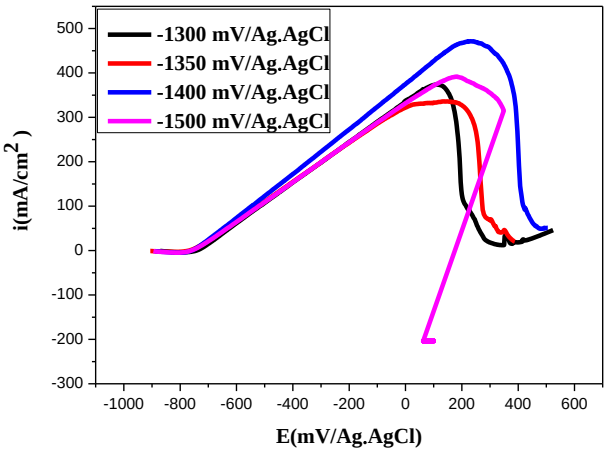

Fig.3. Anode dissolution (ALSV) of synthesized deposits with imposed potential in an electrolyte:ZnCl2 0.15 M, FeCl20.75 M, KCl 180g/L, boric acid 25g/L, 0.02 M L-ascorbic acid, 2g/L « Saccharin», 10-3 M « Glycérol».

3.3. Morphological study of deposits

Observations using the SEM scanning electron microscope allowed to characterize the deposits obtained at different imposed potentials.

Micrographs Fig.4.a and Fig.4.b show the SEM observations of additive deposits in a chloride bath, a very tormented nodular morphology is obtained at – 1300 mV/Ag,AgCl in the presence of saccharin and glycerol.

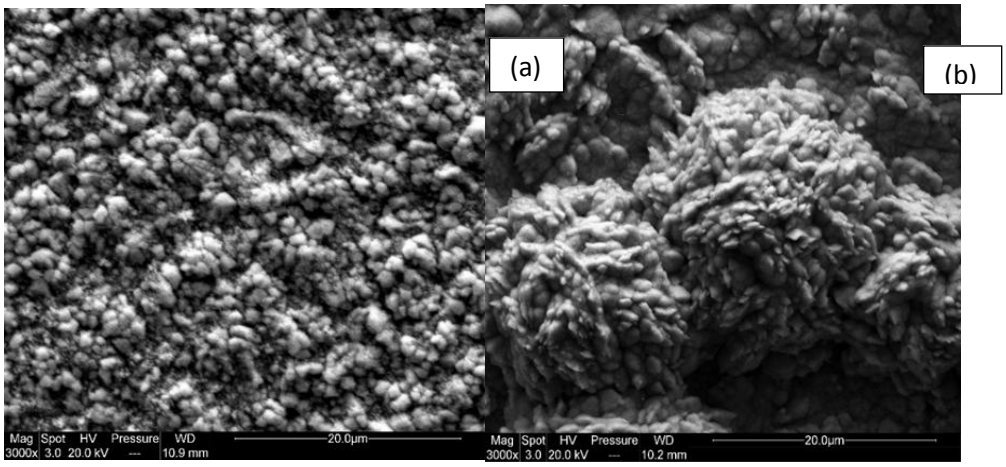

Fig.4. SEM images of E24 steel in E3, (a) without saccharin, (b) in presence of 0.25g/l saccharin.

3.4. Study of corrosion behavior

3.4.1 Potentiodynamic polarization analysis

The deposits made at different potentials and temperature 50°C were immersed in a NaCl bath and were subjected to a corrosion test in a potentiodynamic test. The evolution of the current density as a function of the potential is represented, for each sample on Figure.5 These curves consist of two branches[10,11].: anodic and cathodic. The electrochemical parameters derived from these curves are given in Table .1.

The corrosion current density (icorr) expressed in mA/cm² and which in fact expresses the corrosion rate of the Zn-Fe alloy shows that deposits with better corrosion resistance are those obtained at -1300 and -1400 mV/Ag, AgCl (Table.1).

Fig.5. Potentiodynamic curves of Zn-Fe deposits at different potentials

Table.1: Electrochemical parameters of alloys

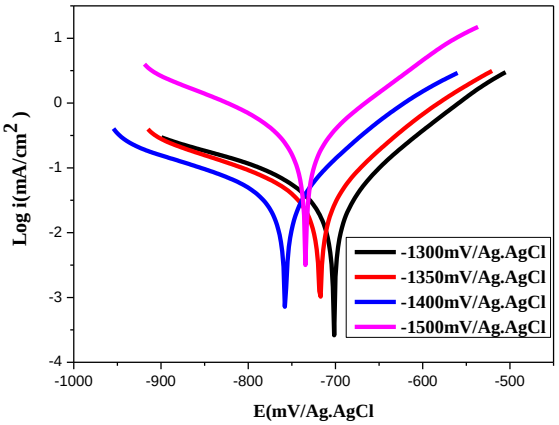

Fig.5. Potentiodynamic curves of Zn-Fe deposits at different potentials

Table.1: Electrochemical parameters of alloys

E (mV/ Ag, AgCl)	Ecorr(mV/ Ag, AgCl)	icorr (mA/cm²)
-1300 mV/Ag.AgCl	-239.204	1.543
-1350 mV/Ag.AgCl	-762.108	0.707
-1400 mV/Ag.AgCl	-715.453	1.202
-1500 mV/Ag.AgCl	-701.934	0.250

3.5. Electrochemical impedance spectroscopy measurements (EIS)

The electrochemical impedance spectra obtained in NaCl 30g/L are represented by Figure 6, which shows the impedance response during the immersion time for various imposed potentials.

The specific parameters obtained by adjustment and calculated using the "EC-lab express demo" Software have enabled the following equivalent circuit to be defined (Fig.6.).

The impedance readings obtained for the Zn-Fe electrolyte and with deposition potential -1300 mV/Ag, AgCl are larger, reflecting a better corrosion resistance compared to those obtained for other coatings, This confirms the results obtained previously[12-15].

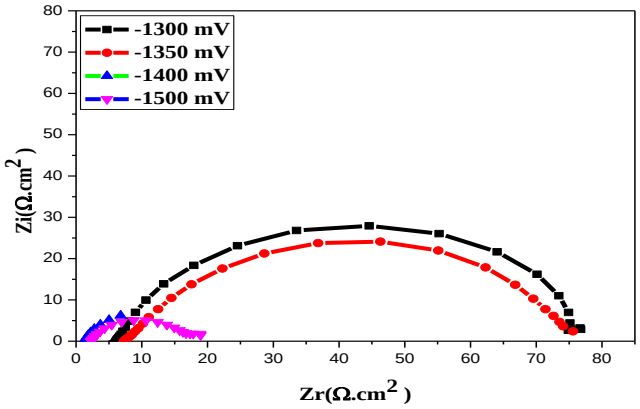

Fig. 6. Nyquist diagrams of Zn-Fe in NaCl 30g/L at different potential imposed at 298 K.

The equivalent electrical circuit (EEC), obtained with the help of a simulation software EC-lab, is shown in Figure 7.

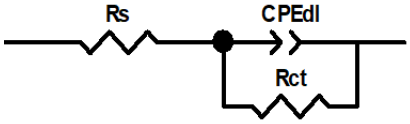

Fig.7. Equivalent electrical circuit of Zn-Fe in NaCl 30g/Lat different potential [16].

The values of the different parameters, taken from the parametric fit are grouped in Table 2.

Table 2. Electrochemical parameters, obtained by EIS, and of Fe, Zn and Zn-Fe steel without and with different concentrations of saccharin.

Elements	Re ($\Omega.cm^2$)	Cdl ($\mu F.cm2).10^{-3}$	α	Rct ($\Omega.cm^2$)
Fe	2.07	0.22	0.70	776
Fe+ 0.25g/l saccharin	1.31	0.82	0.69	68.95

Zn	1.47	0.86	0.69	123
Zn+ 0.25g/l saccharin	1.48	0.84	0.76	51.24
Zn-Fe	1.07	0.15	0.80	291
Zn-Fe+0.25g /l saccharin	1.87	0.11	0.88	1033

The values of these parameters show that: the charge transfer resistance Rct increases up to 1033 $\Omega.cm^2$, this is attributed to the formation of a protective film at the metal/solution interface, [17]; the decrease in Cdl values up to 0.11. 10^{-3} $\mu F.cm^2$ may result from the increase in the thickness of the film formed on the metal surface which may be due to the adsorption of the saccharin molecules at the metal/solution interface or the decrease in the local dielectric constant [18].

4. Surface Analysis

Figure.8. shows the micrographs of the surface of the Zn-Fe alloy, obtained by SEM in E3 in the absence and presence of 0.25g/l of saccharin and at a current density of 2.5 A.dm-^{2}; without additive (Fig. 8(a)), a very tormented nodular type morphology is obtained for the deposit made in the bath; with additive (Fig. 8(b)), it presents a smooth aspect and a considerable refinement of the morphology of the crystals is observed. These results confirm the adsorption of saccharin molecules on the surface of the samples[19,20].

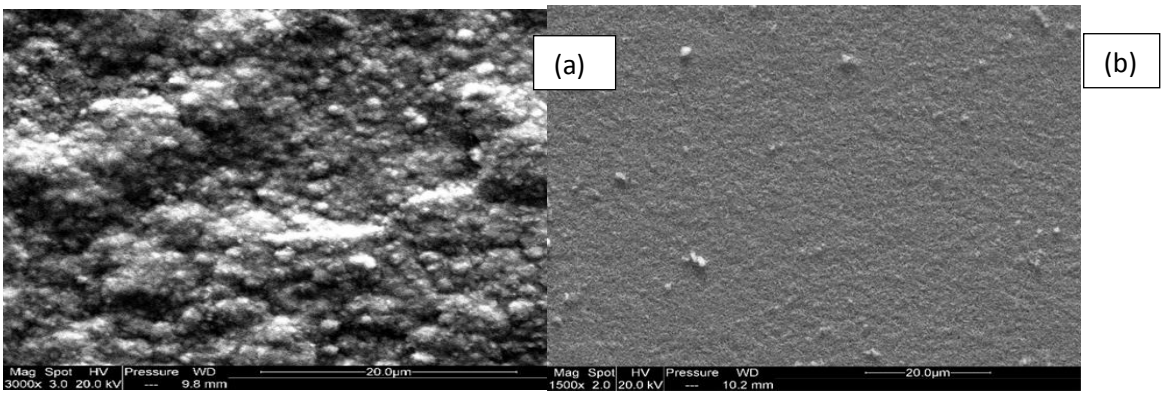

Fig.8. SEM images of E24 steel in E3, (a) without saccharin, (b) in presence of 0.25g/l saccharin.

5. Study of the corrosion products

The X-ray diffractograms of the Zn-Fe alloy recorded on a BRUKER AXS D8 diffractometer are adjusted by Maud software after a potentiodynamic corrosion test (Fig. 9(a, a') and (b, b')), allows to identify the different phases.

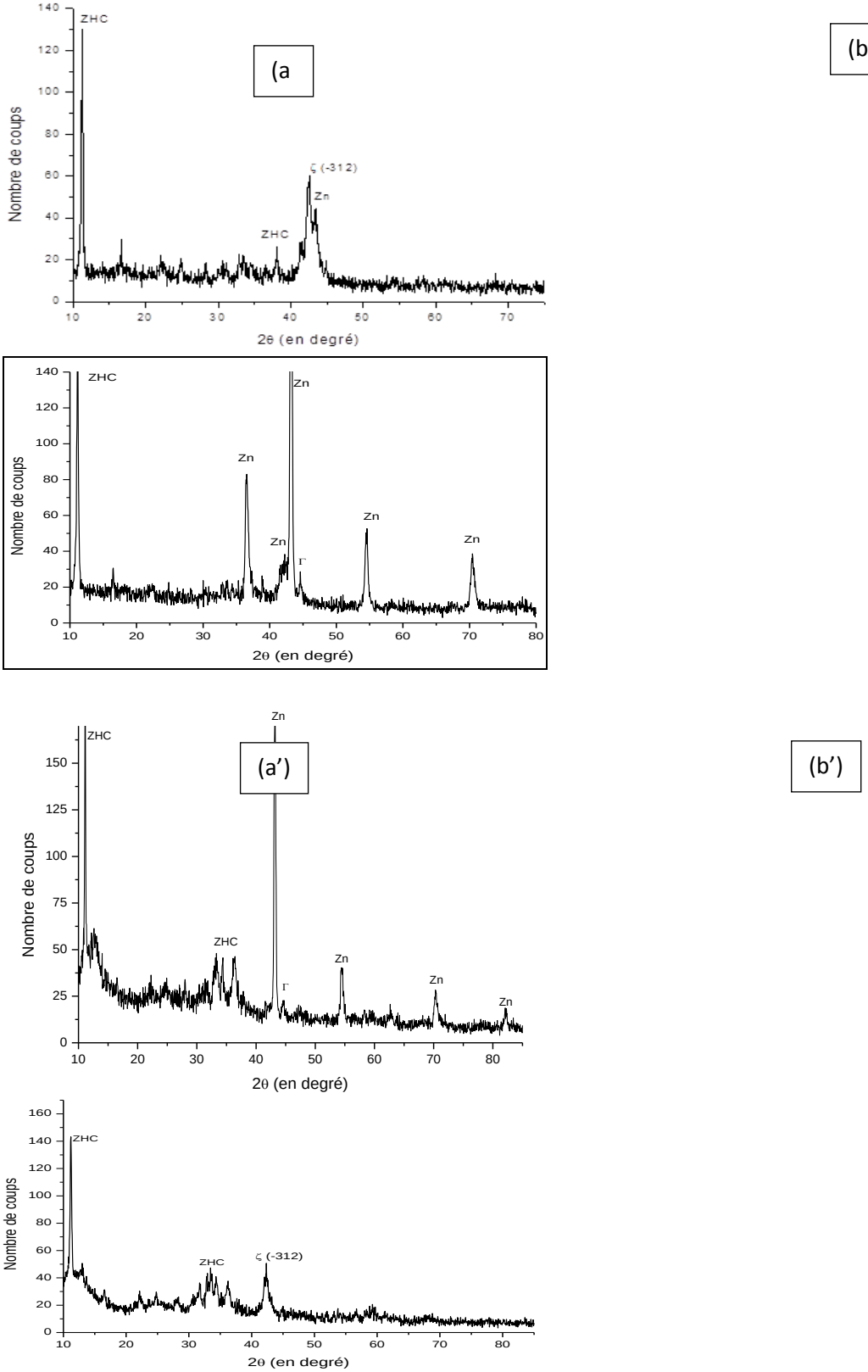

Fig.9. X-ray diffractograms of a Zn-Fe alloy (a,b) deposited at 2.5A/dm^2 ,(a',b') deposited at 1.5A/dm^2 in a bath without and with saccharine subjected to a potentiodynamic corrosion test.

At equal current density, and after subjecting the samples to a potentiodynamic corrosion test, it appears that only one corrosion product can be observed: a zinc chlorohydroxide of the formula $ZnCl_2,4Zn(OH)_2$, denoted ZHC. In the presence of saccharin Fig.9(b), the phases observed for a non-oxidized deposit are found (pure zinc phase and alloy phase) in addition to the ZHC phase.

In the absence of saccharin Fig.9(a), the same ZHC phase is observed but we also observe a phase of the alloy, not present before corrosion . This can be explained by the fact that the X-ray diffraction analysis before corrosion was performed in symmetrical mode while the one after corrosion was performed in fixed and grazing incidence[13].We can thus deduce a certain heterogeneity of the deposit in thickness, the grazing incidence allowing to observe only the superficial layer of the deposit whereas the symmetry mode allows a more in-depth analysis.

After the long term corrosion test, Fig 9 (a' and b'), only the $ZnCl_2,4Zn(OH)_2$ phase (noted ZHC) appears in addition to the phases observed under the same conditions before corrosion. Identical observations can be made for deposits made at a current density of 2.5A.dm^{-2}).

Whatever the corrosion test, long term immersion or potentiodynamic, it seems that the phase has completely disappeared and that the only corrosion product is $ZnCl_2,4Zn(OH)_2$.

It should be noted, however, that other corrosion products are likely to be present without being observable by X-ray diffraction. Indeed, this method allows to observe only the compounds having a crystalline structure, the amorphous compounds are not observable with this technique.

Each sample, after having undergone the various corrosion tests, is analyzed by Raman spectroscopy. The different spectra obtained are presented below, the identification of the peaks was carried out according to [19].

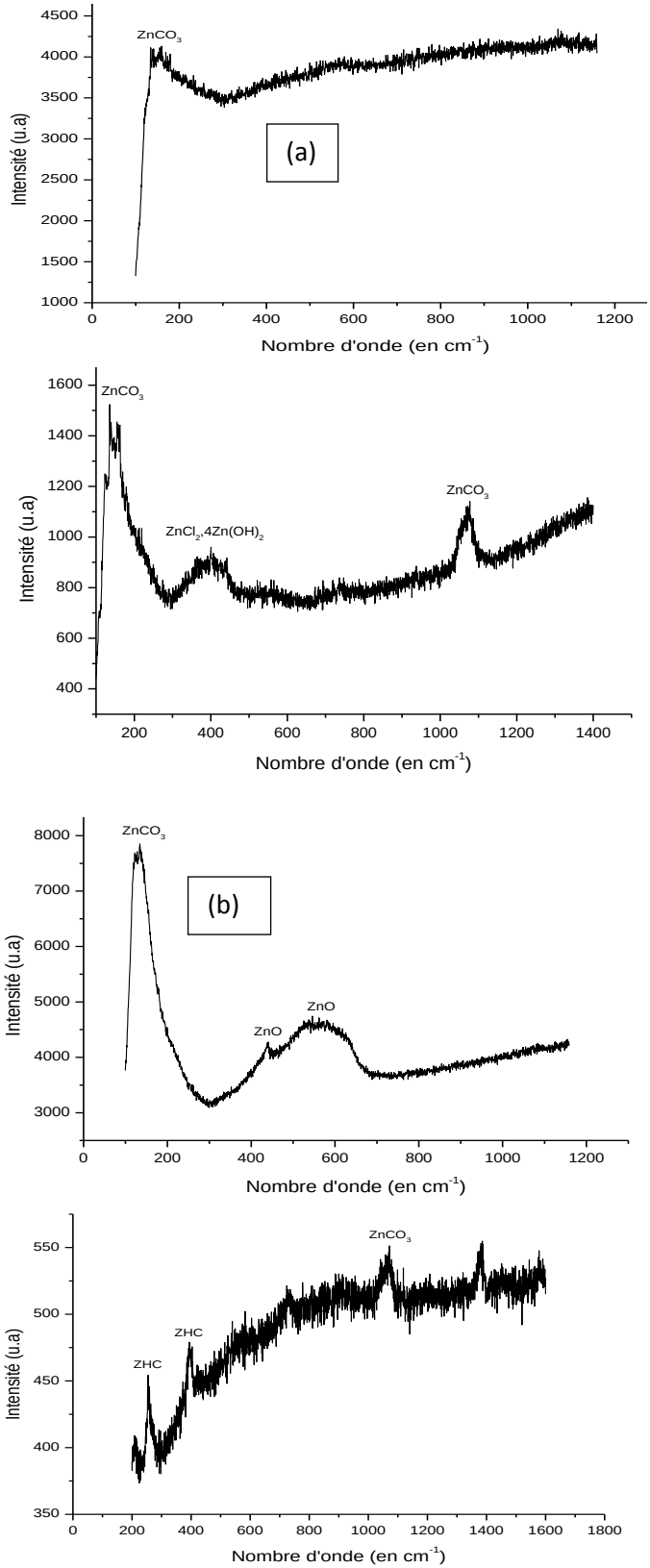

Fig.10. Raman spectra of a Zn-Fe deposit carried out at 1.5 and 2.5 A.dm^{-2} in a bath (a,a') without saccharine, (b,b') in the presence of 0.25g/l saccharine.

From the Raman spectra, the different corrosion products formed during the long immersion can be determined. It follows that in the presence of saccharin (Figure 10 (b,b')), three different corrosion products are obtained: $ZnCO_3$, ZnO and $ZnCl_2$,$4Zn(OH)_2$ (denoted ZHC). Without saccharin, only two corrosion products are present, $ZnCO_3$ and $ZnCl_2$,$4Zn(OH)_2$ (Figure 10 (a,a')). It seems that $ZnCO_3$ and $ZnCl_2$,$4Zn(OH)_2$ are protective in a saline environment but that the presence of ZnO induces a better protection considering the results obtained in potentiodynamics for deposits made in the presence of saccharin. Indeed, these, and in particular the one obtained for a current density of 2.5A.dm^{-2}, have a lower corrosion current density than the deposits obtained for a bath without saccharin. Deposits made in the presence of saccharin would thus present a better protection for the substrate.

5. Conclusion

The study of the early stages of electrocrystallization of Zinc- Iron Alloy on E 24 steel was evaluated by different methods The following insightful conclusions were made;

- Electrodeposition of Zn-Fe on E24 steel follows multiple (3D) nucleation with diffusion-controlled growth following the Scharifkeret Hills model.In fact at potential -1300 mv/Ag, AgCl it follows a theoretical response of instantaneous nucleation according to I^2/Im transients.
- The shapes of the anodic dissolution curves by ALSV of the coatings deposited at different potentials (-1300 -1500 mV/Ag.AgCl) from an electrolyte at 50° C are quite similar and these curves correspond to the dissolution of a single phase (a single step). Moreover, the electrochemical species involved in the dissolution of these coatings (width of the dissolution peak) are very similar, which means that their cathodic efficiencies are fairly constant (quantity deposited/ theoretical quantity).
- Scanning electron microscope observations of the deposits obtained under stationary conditions show a nodular type morphology for the deposits made at -1300mV/ Ag, AgCl.
- The corrosion current density (icorr) expressed in mA/cm^2 and which in fact expresses the corrosion rate of the Zn-Fe alloy shows that the deposits with better corrosion resistance are those obtained at -1300 and -1400 mV/Ag, AgCl (0.250 and 0.707 mA/cm^2).
- The impedance readings obtained for the Zn-Fe electrolyte and at deposition potential -1300 mV/Ag, AgCl have a larger size, reflecting better corrosion resistance compared to those obtained for the other coatings, which which confirms the results obtained previously.
- In perspective, a more in-depth study is essential to identify the best electrodeposition conditions and to define its mechanism.
- Structural and magnetic characterizations are also essential in order to highlight the properties of the material according to the conditions of elaboration.

References

[1] Gabe DR, Green WA Surf Coat Technol;105-195(1998) .

[2] S. Selvakumari , M. Chandran , S. Premlatha, G.N.K. Ramesh Bapu, P. Subramaniam , Effect of Additives on Morphology Texture And Corrosion Resistance of Electrodeposited Zinc And Zinc-Cobalt Alloy International Journal Of Engineering Research And Development e-ISSN: 2278-067X, p-ISSN: 2278-800X, www.ijerd.com Volume 13, Issue 12 (December 2017),21-31.

[3] F. L. G. Silva, Dalva Lago, E. D'Elia, L. F. Senna, Electrodeposition of Cu–Zn alloy coatings from citrate baths containing benzotriazole and cysteine as additives, November 2010 Journal of Applied Electrochemistry 40(11).

[4] M. Missioui, M.B. Idrissi, F. Benhiba, Z. Atioğlu, M. Akkurt, H. Oudda, J.T. Mague, E.M. Essassi, A. Zarrouk, Y. Ramli, Synthesis, structural characterization, Hirshfeld surface analysis and anti-corrosion on mild steel in 1M HCl of ethyl 2-(3-methyl-2-oxo-1, 2-dihydroquinoxaline-1-yl) acetate, Journal of Molecular Structure 1251 (2022) 132047.

[5] I. Nadi, M. Bouanis, F. Benhiba, K. Nohair, A. Nyassi, A. Zarrouk, C. Jama, F. Bentiss, Insights into the inhibition mechanism of 2, 5-bis (4-pyridyl)-1, 3, 4-oxadiazole for carbon steel corrosion in hydrochloric acid pickling via experimental and computational approaches, Journal of Molecular Liquids 342 (2021) 116958.

[6] B. Sameh, B. Baya, B. Louiza, H. Soraya, B. Hatem, B. Merzoug, Corrosion inhibition impact of Pyracantha coccinea M. Roem extracts and their use as additives in zinc electroplating: Coating morphology, electrochemical and weight loss investigations, Journal of the Taiwan Institute of Chemical Engineers 121 (2021) 337-348.

[7] J.-H. Park, K.-P. Ko, T. Hagio, R. Ichino, M.-H. Lee, Effect of Zn-Mg interlayer on the corrosion resistance of multilayer Zn-based coating fabricated by physical vapor deposition process, Corrosion Science 202 (2022) 110330.

[8] S. Anwar, Y. Zhang, F. Khan, Electrochemical behaviour and analysis of Zn and Zn–Ni alloy anti-corrosive coatings deposited from citrate baths, RSC advances 8(51) (2018) 28861-28873.

[9] U.S. Geological Survey.Mineral commodity summaries 2013. U. S. Geological Survey; 2013. p. 188–9.

[10] W. Liu, Q. Li, M.-C. Li, Corrosion behaviour of hot-dip Al–Zn–Si and Al–Zn–Si–3Mg coatings in NaCl solution, Corrosion Science 121 (2017) 72-83.

[11] N. Hosking, M. Ström, P. Shipway, C. Rudd, Corrosion resistance of zinc–magnesium coated steel, Corrosion science 49(9) (2007) 3669-3695.

[12] J.J. Kelly, C. Tian, A.C. West, Leveling and microstructural effects of additives for copper electrodeposition, Journal of the Electrochemical Society 146(7) (1999) 2540.

[13] D. Nam, R. Kim, D. Han, J. Kim, H. Kwon, Effects of (NH4) 2SO4 and BTA on the nanostructure of copper foam prepared by electrodeposition, Electrochimica Acta 56(25) (2011) 9397-9405.

[14] Q. Li, J. Hu, J. Zhang, P. Yang, Y. Hu, M. An, Screening of electroplating additive for improving throwing power of copper pyrophosphate bath via molecular dynamics simulation, Chemical Physics Letters 757 (2020) 137848.

[15] S. Amirat, R. Rehamnia, M. Bordes and J. Creus, Materials and Corrosion, Vol 64, Issue 4, (2013) 328–334.

[16] S. Amirat, R. Rehamnia, M. Bordes and J. Creus, Zn–Fe alloy electrodeposition from chloride bath: Influence of deposition parameters on coatings morphology and structure,Materials and Corrosion, 62,No 9999, (2011) 328–334.

[17] K.Abderrahim, O. Mohammad Ahmad Khamaysa, I.Slatnia and H.Zeghache ,Adsorption and performance assessment of 5-Mercapto-1-Methyl Tetrazole as A9M steel corrosion inhibitor in HCl medium: A detailed experimental, and computational methods, chemical data collections 39 (2022) 100848.

[18] K. Abderrahim, T. Chouchane, I. Selatnia, A. Sid, P. Mosset, Evaluation of the effect of Tetramethylammonium hydroxide on the corrosion inhibition of A9M steel in industrial water: an experimental, morphological and MD simulation insights,chemical data collections 28 (2020) 100391.

[19] K. Abderrahim , I. Selatnia , A. Sid , P. Mosset,1,2-bis(4-chlorobenzylidene)Azine as new and effective corrosion inhibitor for copper in 0.1N HCl: A combined experimental and theoretical approach,chemical physics letters 707 (2018)117-128.

[20] P. B.Raja, A.A. Rahim, H. Osman and K. Awang, Inhibitive effect of Xylopia ferruginea extract on the corrosion of mild steel in 1M HCl medium, Int. J. Miner. Metall. Mater, 18(2011), No.4, p. 413.

[21] I. B.Obot and A.Madhankumar, Synergistic effect of iodide ion addition on the inhibition of mild steel corrosion in 1 M HCl by 3-amino-2-methylbenzylalcohol, Mater. Chem. Phys, 177(2016), p. 266.

[22] A.J.Bard,L.R.Faulkner,Electrochimicalmethods-Fundamental sand applications, JohnWiley&SonsInc.(2001).

[23] L.Humberto Mendoza-Huízar, C.Hilda Rios-Reyes, M. Guadalupe Gómez-VillegasJ. Mex. Zinc Electrodeposition from Chloride Solutions onto Glassy Carbon Electrode Chem. Soc. 2009, 53(4), 243-247.